Journal of Power Sources 260 (2014) 140–149

Contents lists available at ScienceDirect

Journal of Power Sources

journal homepage: www.elsevier.com/locate/jpowsour

Influence of selected coal contaminants on graphitic carbon electro-oxidation for application to the direct carbon fuel cell

John Tulloch [a,b], Jessica Allen [a], Louis Wibberley [b], Scott Donne [a,*]

[a] University of Newcastle, Discipline of Chemistry, Callaghan, NSW 2308, Australia
[b] CSIRO Energy Technology, 10 Murray Dwyer Cct, Mayfield West, NSW 2304, Australia

HIGHLIGHTS

- Anodic carbon electrochemistry in a molten carbonate electrolyte has been examined.
- Anodic oxidation of graphite is enhanced/catalyzed in the presence of mineral clays.
- The mechanism involves a solid phase interaction between the minerals and graphite.
- Clays such as kaolin and montmorillonite modify the carbon oxidation mechanism.

GRAPHICAL ABSTRACT

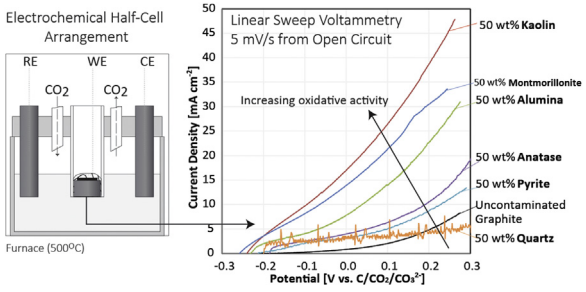

ARTICLE INFO

Article history:
Received 13 December 2013
Received in revised form
10 February 2014
Accepted 5 March 2014
Available online 18 March 2014

Keywords:
Carbon
Direct carbon fuel cell
Electrochemical reactivity
Coal contaminant
Solid-phase interaction

ABSTRACT

A novel method examining the fundamental electrochemical behaviour of carbon is outlined here involving the use of a half cell set-up and solid sacrificial anode. Using this method, electrochemical oxidation of graphite is assessed using selective contamination of a graphite electrode with major coal contaminants identified in selected Australian black coals using X-ray diffraction. Contaminants identified include anatase, alumina, pyrite, quartz, kaolin and montmorillonite. From the systematic introduction of these contaminants it is shown that clay materials, such as kaolin and montmorillonite, act catalytically to increase the rate of graphite oxidation. Metal oxides and sulfides such as anatase, alumina and pyrite give a limited increase in the normalised current, whereas quartz gives a significant decrease in performance. This demonstrates a clear effect of the solid phase interaction of these contaminants on the electrochemical oxidation of graphite since the same effect is not observed when the contaminants are added instead to the molten carbonate electrolyte.

1. Introduction

Fossil fuel-based energy production is neither sustainable nor in good favour with current climatic concerns. Modern energy production is heavily reliant on fossil fuels such as coal, gas and oil, all of which produce emissions such as carbon dioxide (CO_2), nitrogen oxides (NO_x) and sulfur dioxide (SO_2), which interrupt natural cycles and processes. Furthermore, demand for electricity production is globally increasing and many current research interests focus on the design and development of new power generation technologies which also act to reduce emissions intensity. One such technology is the Direct Carbon Fuel Cell (DCFC).

The DCFC produces electrical energy through the reduction of oxygen within the cathode of the cell, with oxidation of the carbon

* Corresponding author. Tel.: +61 2 4921 5477; fax: +61 2 4921 5472.
E-mail addresses: fishinabottle@gmail.com (J. Tulloch), j.allen@newcastle.edu.au (J. Allen), Louis.wibberley@csiro.au (L. Wibberley), scott.donne@newcastle.edu.au (S. Donne).

http://dx.doi.org/10.1016/j.jpowsour.2014.03.026
0378-7753/

fuel source occurring within the anodic side. Half and full-cell reactions are shown in Eqs. (1)–(3);

$$C + 2O^{2-} \rightarrow CO_2 + 4e^- \quad \text{ANODE} \tag{1}$$

$$O_2 + 4e^- \rightarrow 2O^{2-} \quad \text{CATHODE} \tag{2}$$

$$C + O_2 \rightarrow CO_2 \quad \text{OVERALL} \tag{3}$$

Direct carbon fuel cells are a unique type of fuel cell as they have the ability to utilise solid carbon fuel. They are similar in many regards to the molten carbonate fuel cell (MCFC), differing only by fuel type and minor cell design characteristics [1]. Coal, a well-known source of amorphous carbon, is widely used in energy production around the world and has been identified as a candidate for use in the DCFC [1–5]. Carbonaceous material in coal can be transformed directly to electrical energy within the DCFC with high efficiency assuming non-Boudouard conditions; i.e., chemical conversion of carbon through reaction with carbon dioxide at elevated temperatures [2,6]. This direct conversion has the potential to increase electrical conversion efficiency of the energy contained in coal to over 80% (it is theoretically 100% efficient) compared to conventional coal fired power stations operating below 40% [1] since only one energy transformation takes place. In reality, the conversion of the calorific value of the coal into electrical energy may be somewhat lower than 80% efficient as a result of the need to pre-process the coal to remove volatile components.

Kinetics and limitations of the oxidation reaction of carbon to carbon dioxide under different cell conditions and arrangements have been highlighted recently as important avenues for research pertaining to the DCFC [1,7]. There exist a number of cell designs used in recently published literature that give information on the overall electrochemical performance of different carbon materials and cell components under DCFC conditions [8–15]. A relatively smaller number of research groups have focused on the anodic oxidation reaction specifically, including analysis of electrochemical processes at the anodic electrode [3,16,17].

The electrochemical oxidation reaction was studied in this work using graphite as a base through the use of a specifically designed electrochemical test cell. The cell was designed in order to enable testing of a solid anode arrangement rather than suspended carbon, which has been used in previous investigations [3,13,17]. There are a number of drawbacks in investigations using suspended carbon as a basis, primarily the mass transfer limitations of a cell masking other kinetic behaviour of a particular fuel. Further, if a carbon source artificially contaminated with mineral matter is suspended and stirred within a molten salt (electrolyte) for any period, it is likely that the contaminant phase will interact with the molten salt. However, it has been assumed previously that mineral matter remains a part of the carbon material and affects the reactions on the surface of the particle [3].

Graphitic carbon was chosen for the basis of the study as it represents significantly less variability in carbon type, surface functionalities, ash content and chemistry, and general physical and chemical behaviour compared to other carbon materials tested for use in the DCFC [8,16,18]. Basic oxidative behaviour of graphite was established in order to compare the effect of different contaminants on the oxidation of graphitic carbon.

Contaminants for investigation were chosen based on those present in coal samples. Coal contains a significant amount of mineral matter, commonly in the form of clays, mixed metal and non-metal oxides and pyrite, some of which have been shown to affect the electrochemical oxidation of carbon within test DCFC cells in the form of coal ash [19]. In this work, four Australian bituminous coals (sourced from the Hunter Valley region) and an American coking coal were analysed using XRD to identify mineral phases which exist in significant concentration within the coals studied. Particular care was made to identify contaminants present in the coal as it will be introduced to a DCFC system rather those identified following high temperature ashing—which is known to affect chemical structure of contaminants and coals [20–22].

2. Experimental

2.1. Coal characterisation and treatment

2.1.1. Proximate analysis of coals investigated

Proximate analysis on the coal materials used the method ATSM D3175-11. Ash analysis was also performed on the coals using ASTM D4326-11.

2.1.2. Low temperature ashing

Low temperature ashing was performed in an oxygen plasma low-temperature asher (PE-100, Plasma Etch, Carson City, NV) with an RF power supply providing 200–240 W at frequencies necessary to provide a sustained oxygen plasma (~13.65 MHz). Selected, pre-dried (at 368 K), 20–30 g samples were evenly distributed on 150 mm Pyrex dishes and loaded into the ashing chamber, which was then evacuated to 0.15 Torr. Maintenance of the low-pressure oxygen (BOC industrial grade) atmosphere was through a bleed line (5–30 mL min^{-1}) and a scavenging vacuum pump. Samples were reweighed and gently overturned every 48 h period. Ashing was assumed complete when the mass loss was no greater than 5 mg after a 48 h cycle, complete ashing was observed after 3 weeks. After completion, samples were sealed in airtight containers until further analysis.

2.1.3. Structural analysis

X-ray diffraction (XRD) patterns for selected samples were recorded using a diffractometer (PW-170, Philips). Cu Kα radiation (1.5418 Å) was used to analyse the sample at room temperature using settings of 40 mA and 40 kV, 2θ range of 10°–90°, step size of 0.05° 2θ, scan step time of 2 s, divergence slit–receiving slit–scatter slit widths of 1°–0.2°–1°, respectively.

2.1.4. Morphological analysis

Scanning electron microscopy (SEM) of manufactured electrode surfaces was carried out. To enable microscopic examination of the pelleted carbon samples, a polished specimen was prepared. This was achieved by initially mounting the carbon pellets under pressure in a two-part, cold setting, epoxy resin. The sample was then ground using various grades of silicon carbide paper on a rotating turn-table and finally polished using diamond and silica compounds. This resulted in a relatively flat, representative cross-section, making microscopic examination possible. For SEM examination the sample was mounted on an aluminium stub and carbon evaporation was carried out with a 20 nm conductive layer of carbon suitable for imaging and elemental X-ray analysis. SEM images were taken on a Zeiss MA15 instrument with a silicon drift X-ray detector (SDD) and a back-scattered electron (BSE) detector.

2.2. Working electrode fabrication and selective contamination

2.2.1. Graphite pellet preparation

Graphite (SFG15; Timcal Timrex®, Switzerland) pellets were manufactured in a 13 mm diameter pellet press and compressed at 740 MPa for 5 min. To ensure stability under test conditions, the graphite pellets were then sintered for 4 h under a nitrogen atmosphere at 773 K with no observable changes in appearance or

mechanical strength. Following sintering, the resistivity of the graphite pellets was measured and found to range from 8.0 to 9.3 μΩm.

2.2.2. Contaminated graphite pellet preparation

The particle size of the contaminants was kept below a standard size by dry-milling the mineral phases and passing them through a 40 μm test sieve prior to mixing with the graphite material. Kaolin was further heat treated at 773 K for 30 min prior to pelletising in order to minimise possible mechanical damage to pellets during electrochemical testing as a result of dehydroxylation of kaolin to metakaolin at elevated temperatures [23].

After sieving, contaminants were slowly introduced to the graphite powder while mixing in a mortar and pestle and combined for a further 5 min or until a homogenous powder was produced. Pellets were then prepared identically to pure graphite.

Contaminant materials including alumina (Al_2O_3), quartz (SiO_2) and anatase (TiO_2) were sourced from reputable chemical supplier (Sigma Aldrich), while kaolin, montmorillonite and pyrite were sourced from mineral deposits in the Hunter Valley region of Australia. To confirm their identity and the purity of the contaminant mineral phases sourced, all contaminants were analysed by XRD. All materials were found to match pure references of the material (found in Inorganic Crystal Structure Database) with minor deviations. Deviations observed include the presence of a very minor rutile phase within the anatase and minor traces of quartz in the pyrite material.

2.2.3. Electrode construction

Contact to the carbon pellet was made through a chromel wire cemented in place with a conductive ceramic adhesive (Resbond 989, mixed with 15 wt% graphite). The conductive adhesive, pellet and wire contact were allowed to dry at room temperature for 4 h after which they were heated in a nitrogen atmosphere to 363 K, 393 K and 573 K for 2 h, 1 h and 1 h, respectively, to dry, cure and post cure the adhesive. The carbon pellet and contact were then mounted into a ceramic tube, cemented and cured in place using ceramic adhesive (Resbond 989) using the same procedure as the conductive glue curing. A general arrangement diagram of the anode is shown in Fig. 1.

The surface of the working electrode was polished flat on 1000 grit carbide abrasive paper and well rinsed with Milli-Q water to remove any surface contaminant. This procedure produced a working electrode with a cross sectional geometric area of 1.766 cm^2 (allowing for surface roughness), which has been used to normalise currents recorded in electrochemical testing (along with normalisation used for active carbon surface area as discussed in Section 3.4).

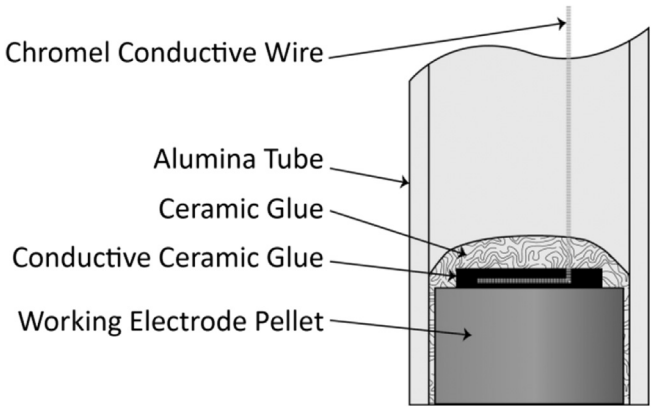

Fig. 1. Anode arrangement.

2.3. Electrochemical cell set-up and testing

Electrochemical experimentation conducted in this work was performed using a potentiostate/galvanostat (273A, Princeton Applied Research PAR, Oak Ridge TN, USA). M270 electrochemical research software was supplied by PAR to control the potentiostat/galvanostat through a high speed-USB general purpose interface bus (GPIB-USB-HS).

2.3.1. Electrochemical arrangement

A three-electrode high temperature electrochemical test cell was manufactured for the purpose of testing the pellets in a molten carbonate eutectic electrolyte. The cell was constructed of high-density alumina (ceramic), prepared and machined by Ceramic Oxide Fabricators (Melbourne, Australia). The cell consisted of a circular ceramic dish with a machined flat top, and a specially manufactured ceramic tile lid to allow the working (WE), reference (RE) and counter (CE) electrodes to be held securely in place. A constant carbon dioxide (BOC grade 4.5) atmosphere was maintained within the cell via an external gas feed line flowing at a rate of 50 $mL_N\ min^{-1}$ in order to maintain constant reference electrode conditions. A temperature of 773 K was used for all experiments. A schematic of the test cell design and setup is shown in Fig. 2.

2.3.2. Electrodes

The counter electrode consisted of a graphite rod (GrafTech, Cleveland OH, USA) with electrical contact through an internally cemented chromel wire (conductive ceramic adhesive and curing regime as above). The graphite electrode was cleaned in 30% HNO_3, rinsed with Milli-Q water and heated to 500 °C under nitrogen to remove any residues from manufacture. The geometric surface area of the counter electrode was approximately 3.7 times that of the working electrode (based on an electrolyte depth of 15 mm), ensuring that any surface area limitations were not a result of the counter electrode.

2.3.3. Tertiary carbonate electrolyte

Sodium carbonate (Na_2CO_3), lithium carbonate (Li_2CO_3) and potassium carbonate (K_2CO_3) (Sigma >99% pure) were dried at 110 °C under vacuum for 24 h prior to combining. The three carbonate powders were combined in a mole ratio of 43.5% Li, 31.5% Na, 25% K (m.p. 397 °C [24]) and gently milled with a mortar and

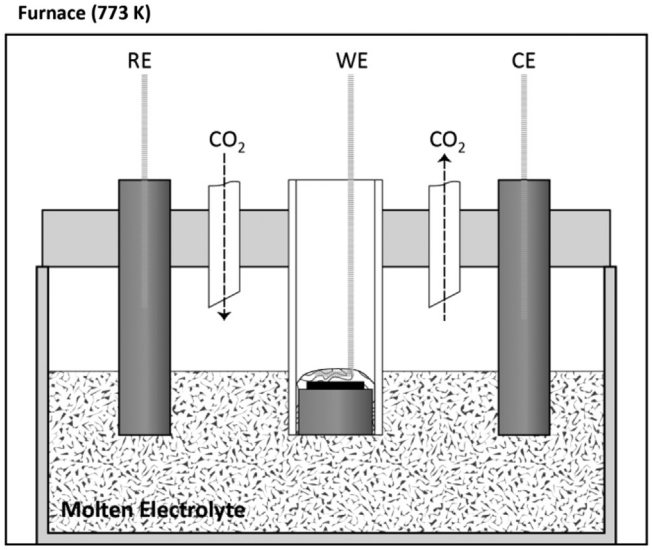

Fig. 2. Electrochemical anodic half cell arrangement.

pestle for 5 min. The tertiary carbonate precursor was then redried at 110 °C for 1 h and treated at 450 °C for 30 min in a platinum crucible under a CO_2 (BOC grade 4.5) atmosphere to form the three component eutectic.

3. Results

3.1. Proximate and ash analysis results

Table 1 summarises the results from the proximate analysis on the five coal samples on a dry basis. From the low ash content and high fixed carbon evident from the proximate analysis it is clear that the Coal-C sample has been processed to remove some of the ash producing phases. All of the other coal materials showed typical proximate analysis results for bituminous coals.

As is commonplace, the elemental composition of the coal ashes were reported as oxides with composition indicated on a weight percentage basis, results shown in Table 2.

Results in Table 2 suggest all coal ashes are dominated by silica with significant inclusion of alumina and ferric oxides. Other constituents are minor and, combined; consist of less than ten per cent of the total ash. Coal-C again is shown to be different from other coals with notably smaller concentrations of silica, alumina and iron oxides—suggesting a preferential removal of these species in the pre-treatment process.

3.2. Identification of coal mineral phases of interest

Raw coals (proximate analysis provided in Table 1) were analysed using XRD. Results are shown in Fig. 3[A] along with XRD patterns for coals which have undergone the LTA procedure outlined in Section 2.1.2 (Fig. 3[B]).

All of the raw coal materials showed two broad peaks in the range 10–30°2θ and 30–60°2θ which are known to be characteristic of poorly crystalline carbon materials [3,25]. Superimposed on the broad carbon peak there are several peaks from the crystalline mineral matter in the raw coal samples; namely kaolin (denoted with κ in Fig. 3) and quartz (denoted with θ), with kaolin peaks at 12.1°2θ, 24.5°2θ and distinct multiple peaks at 20.5°2θ. The peaks due to quartz, 20.45°2θ and 26.4°2θ, are distinct for all the raw coal materials with the main quartz peak, 20.45°2θ, giving the largest peak in all the raw coal patterns. This peak from the quartz phase is exaggerated somewhat as the graphitic carbon in the coal material also has a main peak at 26.15°2θ. However, the secondary peaks at 49.3°2θ and 59.4°2θ confirm the presence of the quartz phase in the raw coals. In the case of Coal-D these secondary quartz peaks are minor peaks in the background, likely due to the fact that the majority of the quartz in the Coal-D raw coal is tied up in the clay materials in the sample. The XRD pattern of the raw Coal-D sample also showed small peaks at 32.55°, 36.5°, 40.35°, 46.95° and 55.8°2θ, which are the distinct major peaks from a pyrite (denoted with π) phase in the raw coal.

The large amorphous carbon peaks in the pattern can overshadow many peaks from other mineral phases, meaning detailed information on the mineral phases present in the sample is difficult to establish. LTA was used to remove the carbon material in coal whilst preserving the mineral phases present in the samples through significantly reducing the severity of the ashing temperature and oxidative conditions. XRD patterns from LTA residues collected for each coal sample are shown in Fig. 3[B].

The low temperature ash XRD patterns closely resemble that of their parent coal material with the shadowing broad carbon distortion removed. All of the patterns show strong kaolin peaks at 12.1°2θ and 24.7°2θ, and multiple peaks at 19.9°2θ and 38.1°2θ. A large quartz peak can be observed clearly at 26.4°2θ and minor peaks at 20.5°, 36.1°, 49.8° and 67.5°2θ are also evident. It is apparent from these features that the low temperature ashing has not disrupted the mineral phases present in the coal samples.

In comparing the Coal-C and Coal-E raw coal and LTA residue XRD results, it was apparent that the beneficiation process used on the Coal-C sample, whilst decreasing the overall mineral content of the coal sample, shows preference for the removal of certain phases. Evidence for this is the lack of any well-defined clay (kaolin) peaks in the Coal-C pattern, along with the significant reduction in peak height from the quartz mineral phase. From the proximate analysis the Coal-C and Coal-E coals both showed a high Si:Al ratio, indicating that there was likely to be a higher quartz phase present in these samples. Coal-E shows strong primary and secondary peaks from a quartz phase, whereas the secondary quartz peaks are almost lost in the background for the Coal-C raw coal spectra. From the XPert analysis software, only quartz and polymorphic graphite were identified in Coal-C.

It is evident from this analysis that the coal materials have a wider range of mineral chemistry than the basic oxides reported in the proximate analysis in Section 2.1.1. Through the use of both SiroQuant and XPert XRD analysis software a multitude of mineral phases were identified in these LTA samples. Table 3 highlights the range of mineral phases found in these LTA residues.

Quartz and anatase were the only significant oxide phases found in the LTA samples. This result is strongly supported by Ward [27] who also determined that the only significant oxides found in a compilation of LTA results were quartz (SiO_2) and anatase (TiO_2). This result illustrates that testing the effects of coal contaminants as they are likely to be introduced to the DCFC requires addition of the significant mineral phases and not their oxide counterparts.

3.3. Graphite performance, stability and reproducibility

In order to determine the performance of graphite as a baseline pressed pellet in the novel electrode design, several test methods were used to confirm its oxidative performance and reproducibility without addition of electrode contaminants. The graphite working electrode (prepared using procedure outlined in Section 2.2.1) was used in the assembled test cell along with the graphite rod counter and reference electrodes with the standard carbonate eutectic.

Due to the sacrificial nature of the carbon electrode pellet fabricated, it was determined to be important to test the continued electrochemical performance over a series of successive electrochemical sweeps. This was done to ensure no degradation in performance occurred for the time frame required to perform electrochemical testing.

Table 1
Proximate Analysis of Coals Used in Study (w/w% on a dry basis).

Sample	Ash [w/w% (db)]	Volatile matter [w/w% (db)]	Fixed carbon [w/w% (db)]
COAL-A (Hunter Valley AU)	10.1	35.3	54.6
COAL-B (Hunter Valley AU)	8.7	34.9	56.4
COAL-C (Hunter Valley AU)	2.3	35.1	62.6
COAL-D (Pittsburgh US)	9.3	37.9	52.8
COAL-E (Hunter Valley AU)	11.5	34.2	54.3

Table 2
Ash constituent analysis (wt%) of coals.

	SiO_2	Al_2O_3	Fe_2O_3	TiO_2	Na_2O	CaO	SO_3	K_2O	MgO
COAL-A	56.5	27.6	6.4	1.4	1.3	1.5	2.1	1.2	0.9
COAL-B	58.2	27.4	4.6	1.3	3.8	0.9	1.2	1.5	0.8
COAL-C	73.5	14.8	1.7	4.8	0.6	0.6	0.2	1.1	0.4
COAL-D	41.6	23.5	20.3	1.1	0.8	5.4	3.5	1.7	1
COAL-E	72.4	14.6	5.8	0.1	3.6	0.9	1.2	0.6	0.7

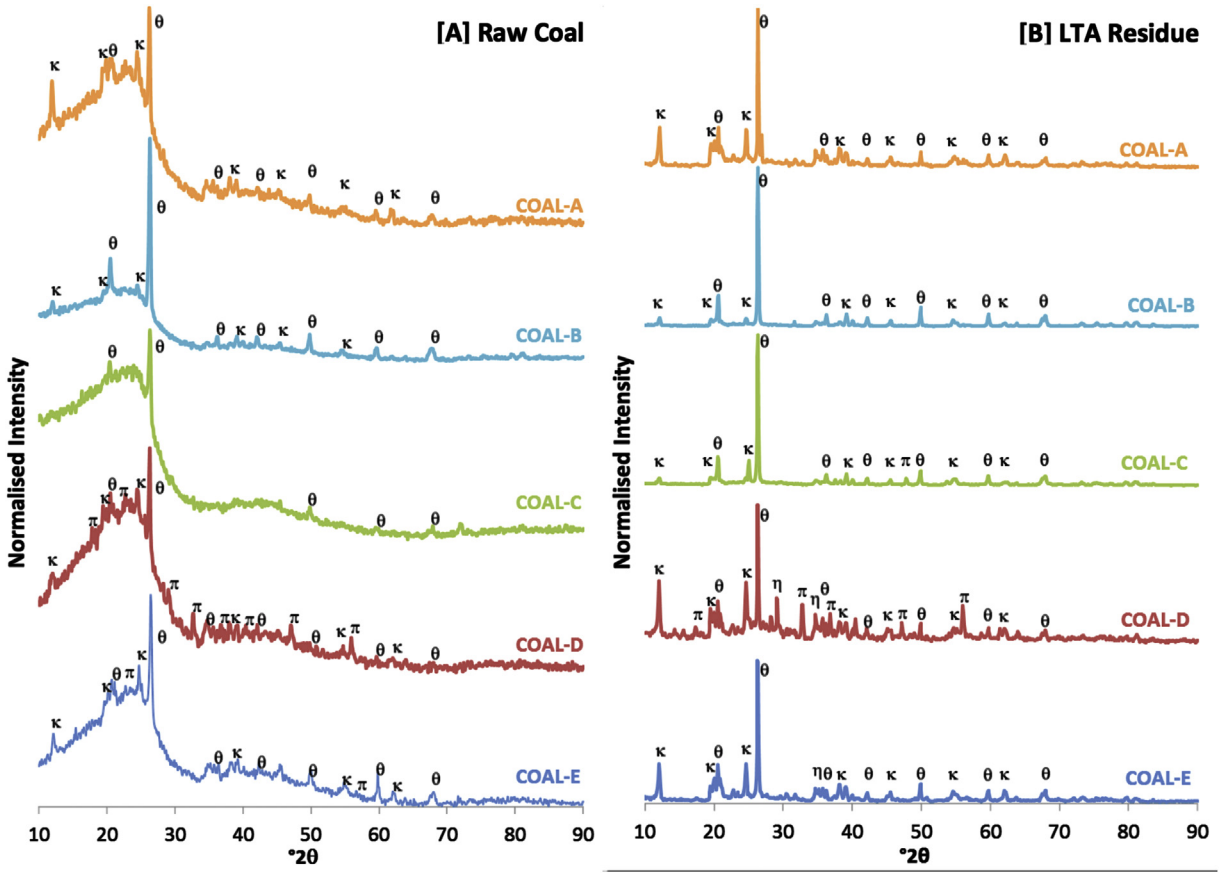

Fig. 3. XRD patterns from [A] raw coal and [B] LTA residues (κ—kaolin, θ—quartz, π—pyrite).

Once the cell was prepared, as shown in Fig. 2, it was heated to 773 K and allowed to equilibrate for 30 min. Following equilibration, numerous potential sweeps were made over the selected potential range; i.e., from the open circuit potential (OCP) of the cell to 0.5 V above the OCP versus the $C/CO_2/CO_3^{2-}$ reference. A scan rate of 5 mV s^{-1} was employed over a 30 min period. This equated to 10 consecutive potential sweeps with a 60 s rest interval between each scan. The anodic response over the course of this experiment is shown in Fig. 4.

Fig. 4 shows almost identical i–V curves for each repeated scan, indicating that the electrochemical behaviour using a graphite solid anode is reproducible and consistent over multiple scans. There is a small amount of variation seen in the i–V curves, most likely due to changes in the electrode surface from consumption of the carbon material from each successive potential sweep. Since the oxidation does not depend on the mass transport of carbon to the electrode surface as with particulate type cells, no mass transport limitations are observed in Fig. 4. This also suggests the diffusion of the CO_3^{2-} species from the electrolyte bulk to the electrode-electrolyte interface is not limiting since, in the half-cell system, the anodic reaction also depends on the presence of carbonate; i.e.,

$$C + 2CO_3^{2-} \rightarrow 3CO_2 + 4e^- \quad \text{ANODE} \tag{4}$$

The diffusion coefficients of the carbonate anion, 0.85–1.92 $\times$ 10^{-5} cm^2 s^{-1}, in mixed alkali salts under various thermal conditions are reported in a wide range of literature [28–31]. However, within the electrochemical environment; i.e., under conditions where there exists a potential gradient, the diffusivity of ions can behave significantly differently. Costa et al. [32] report, on average, a 40% increase in the diffusion coefficient for the CO_3^{2-} ions in mixed alkali carbonate molten salts under an applied

Table 3
Identified mineral phases in the LTA samples of some of the coal materials.

Coal-A		
Quartz $\{SiO_2\}$	Pyrite $\{FeS_2\}$	Fluorapatite $\{Ca_5(PO_4)_3F\}$
Kaolin $\{Al_2Si_2O_5(OH)_4\}$	Calcium Sulfide [26]	Muscovite $\{KAl_2(Si_3Al)O_{10}(F,OH)_2\}$
Montmorillonite $\{Na_{0.3}(Al,Mg)_2Si_4O_{10}(OH)_2 \cdot H_2O\}$	Albite $\{Na(AlSi_3O_8)\}$	Illite $\{KAl_2(Si_3Al)O_{10}(OH)_2\}$
Jarosite $\{KFe_3(SO_4)_2(OH)_6\}$	Siderite $\{FeCO_3\}$	Dolomite $\{CaMg(CO_3)_2\}$
Coal-D		
Kaolin $\{Al_2Si_2O_5(OH)_4\}$	Quartz $\{SiO_2\}$	Pyrite $\{FeS_2\}$
Muscovite $\{KAl_2(Si_3Al)O_{10}(OH)_2\}$	Calcite $\{CaCO_3\}$	Illite $\{KAl_2(Si_3Al)O_{10}(OH)_2\}$
Coal-E		
Quartz $\{SiO_2\}$	Bassanite $\{CaSO_4\ 2H_2O\}$	Kaolin $\{Al_2Si_2O_5(OH)_4\}$
Illite $\{KAl_2(Si_3Al)O_{10}(OH)_2\}$	Calcium Sulfide [26]	Muscovite $\{KAl_2(Si_3Al)O_{10}(F,OH)_2\}$
Dolomite $\{CaMg(CO_3)_2\}$	Haematite $\{Fe_2O_3\}$	

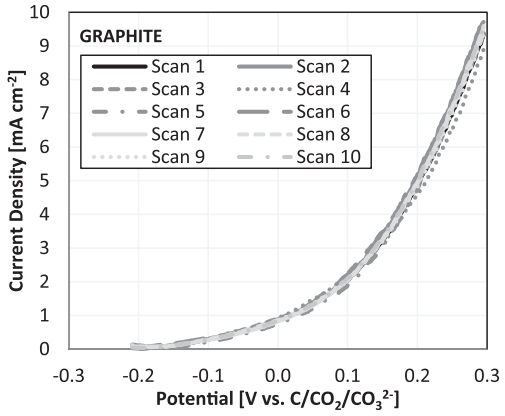

Fig. 4. Repeated LSV performed on graphite (pure) electrode at 5 mV s^{-1} with 60 s interval between scans.

potential gradient. Costa et al. report diffusion coefficients in the range of 3.0–4.7 × 10^{-5} cm^2 s^{-1}. This significant increase in diffusivity, coupled with the fact that the carbonate ionic species constitute near 33% of the mole fraction of the molten electrolyte, accounts for the lack of diffusion-limited behaviour despite quiescent conditions within the cell. The reaction is therefore kinetically limited.

In order to confirm repeatability of experiments where minor differences in preparation of the working electrode where differences in grinding, pelletising and surface treatment of graphite could occur, several electrodes were fabricated using identical methods and tested in the half cell system. The electrochemical test procedure used included determination of the open circuit potential of the system and three subsequent linear sweeps at 5 mV s^{-1} to +0.5 V of the OCP measured (a wait time of 60 s was used between scans, similar to Fig. 4). The OCP and maximum current density at 0.3 V vs. $C/CO_2/CO_3^{2-}$ (average of three sweeps conducted) for each electrode replicate are shown in Fig. 5.

It can be seen in Fig. 5 that the electrochemical results from electrodes manufactured from the same carbon source gave reproducible and consistent results. The average OCP was found to be −0.224 ± 0.003 V vs. $C/CO_2/CO_3^{2-}$ with current density at 0.3 V averaging 9.33 ± 0.49 mA cm^{-2}. This is despite possible small deviations in the final surface topography which may result from the manual electrode preparation method used.

Results shown in Figs. 4 and 5 show good electrochemical reproducibility and stability for a graphite electrode base across which further contamination studies can be performed.

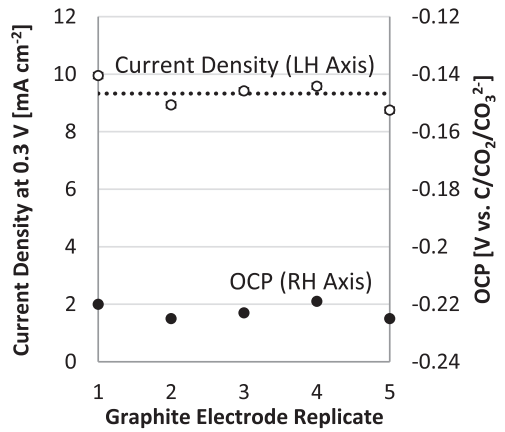

Fig. 5. Electrochemical test results of replicate graphite working electrodes showing OCP (right axis) and current density at 0.3 V vs. $C/CO_2/CO_3^{2-}$ (left axis).

3.4. Selective contamination of graphite electrode

From XRD and proximate analysis results (see Sections 4.1 and 4.2) on the original coal samples used in this study, and their low temperature residues, it was evident that quartz, clay (kaolin and montmorillonite in particular) and pyrite were amongst the more commonly found contaminant mineral phases. Mineral phases also present in high concentrations in the high temperature ash analysis (see Table 2) include anatase and alumina, which were also selected for contamination studies.

Contaminant concentrations between 10 and 50 wt% with graphite were tested using the same electrochemical procedure as described for Figs. 4 and 5 with the third consecutive LSV used as a representative scan. Results for all contaminants tested with various contaminant loadings are shown in Fig. 6 with a comparison of the achievable current density at two different applied potentials included in Fig. 7.

Current density has been normalised in Figs. 6 and 7 to reflect the relative surface area of active graphite present at the electrode surface for each contaminant loading. As the amount of contaminant increases, the active area available for electrochemical oxidation decreases and therefore the reaction occurs on a reduced surface area (contaminants are assumed to be electrochemically inactive in the potential range investigated). The normalisation was carried out by calculating the volumetric weighting of each contaminant based on their density and the density of solid graphite. The geometric surface area used to normalise current per unit area was then changed to reflect the relative volumetric proportion of carbon present. This enables assessment of the current produced per unit area of graphite rather than the total surface area exposed to electrolyte.

SEM was carried out on the surface of each electrode material prior to electrochemical testing in order to confirm homogenization at the electrode surface and the normalization method used. Results, shown in Fig. 8, show some differences in the distribution of contaminants within the graphite electrode.

A 500× magnification was used in each case for comparison of the contaminant phases. SEM images of the surface of the 50 wt% contaminated electrodes confirm that the contaminants are intimately mixed within the graphite material in all cases. However, clear differences in the surface structure are observed dependent on the type of contaminant used.

Kaolin (Fig. 8[A]) appears to be the most intimately mixed of the contaminants with high dispersion in the graphite. It can be seen that the kaolin contaminant has a particle size in the range of 3–8 μm. However, due to some agglomeration, some 'kaolin rich domains' can be as large as 25 μm. It is likely that the conversion of the kaolin to metakaolin caused a reduction in the particle size and the hardness of the kaolin material, resulting in a more finely and evenly dispersed contaminant from the milling step used to introduce the contaminant into the graphite. Very similar results to that of kaolin were found for montmorillonite.

Quartz and alumina (Fig. 8[E] and [B], respectively) appear to be similar in particle size and dispersion, although more graphite rich areas are observed in the case of the alumina. These particulates have a distribution of particle sizes from 4 to 5 μm up to ~45 μm, although average particle sizes appear to rest mostly in the 10–20 μm range.

The anatase contaminant formed larger agglomerated regions, as well as small finely divided particles (see Fig. 8[C]). It is probable that the "marbling" type effect seen in the SEM images is a result of the preparation method used for the SEM. Preparations of the surface of the electrode for the SEM required wet polishing with a very fine abrasive, which would tend to remove the softer graphite material more easily from the surface and smear the anatase into the resulting cavities and clefts. What is evident from the SEM

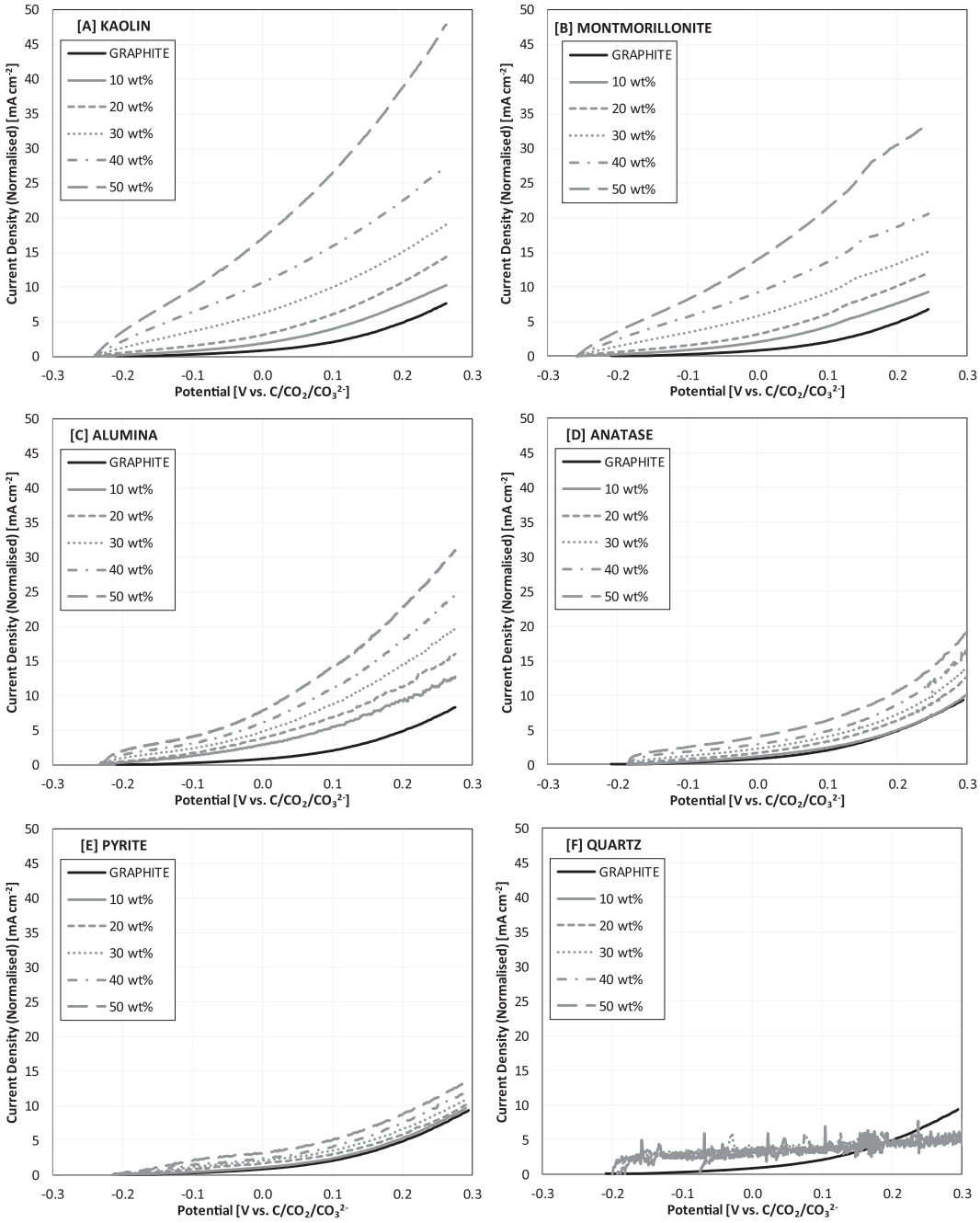

Fig. 6. Electrochemical response for graphite contaminated with [A] kaolin, [B] montmorillonite, [C] alumina [D] anatase, [E] pyrite, and [F] quartz.

images of the anatase contaminated electrode is the clear difference between a contaminant phase that is significantly smaller than the graphite phase percolating through the graphite particles, rather than the graphite particles percolating through the contaminant phase.

Pyrite shows the largest relative particle sizes and therefore the lowest contact between the graphite and contaminant. Pyrite was one of the hardest contaminants (6.5–7 mohs scale) and the grinding process used to reduce the particle size of the pyrite material resulted in a large range of particle sizes varying from 3 to 32 μm with a large incidence of particles in the upper range. As a consequence, the pyrite contaminant was expected to have a larger non-uniform particle size distribution compared to the other contaminants within the working electrodes.

The normalisation technique used is therefore thought to over-represent graphite in the case of anatase (current density is likely larger than appears) while under-representing graphite in the case of pyrite addition (current density is likely smaller than shown through normalisation), however in the majority of cases it is a good approximation for determining the active surface area. It can be seen from Figs. 6 and 7 that with this normalisation, addition of contaminants to electrodes have a significant effect on the reaction which generally increases with additions of the contaminant.

3.5. Contamination of carbonate electrolyte

Complementary to studying the electrochemical effects of contaminating the graphite working electrode, contamination of

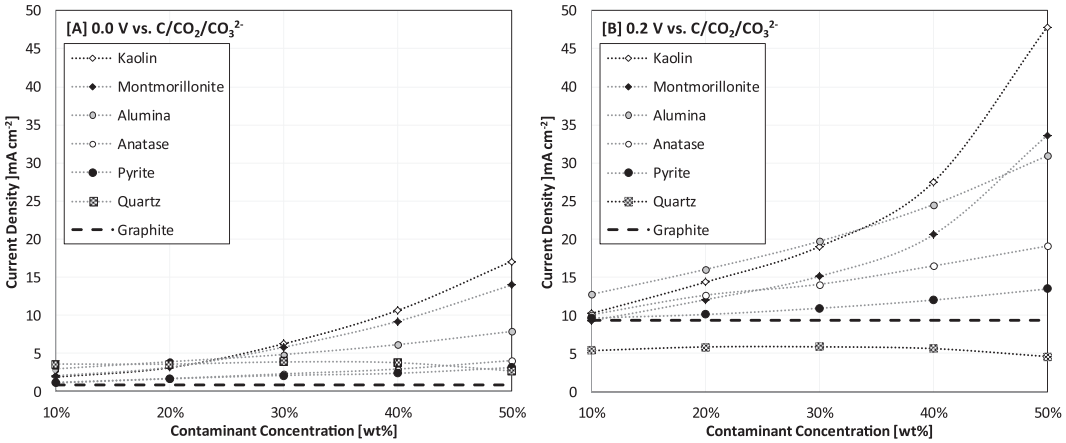

Fig. 7. Comparative performance of graphite incorporated with different contaminants (indicated in figure) with current density measured at [A] 0.0 V vs. $C/CO_2/CO_3^{2-}$ and [B] 0.2 V vs. $C/CO_2/CO_3^{2-}$.

the electrolyte was also undertaken leaving the anode as solid graphite. The electrolyte was then purposefully contaminated with kaolin, montmorillonite, anatase, alumina, pyrite and quartz. Contamination studies were performed for the addition of both 1 and 5 wt% of contaminant to the electrolyte. The same electrochemical procedure as previously described in Section 3.4 was used to evaluate electrochemical performance of the graphite in the presence of the now liquid phase based coal based contaminants.

In contrast to addition of contaminants to the electrode, it was found that for almost all contaminants tested in the electrolyte no discernible change in the current response was seen for graphite electro-oxidation. Differences between LSV curves obtained were no more than normal variation in electrode fabrication procedure as shown in Fig. 4. The only contaminant which did show a small change in LSV behaviour was the quartz contaminant. Both the 1 and 5 wt% contaminant loadings had an effect on the i–V curve from the graphite working electrode at a scan rate of 5 mV s^{-1}, as shown in Fig. 9.

A distinctive feature that can be seen in the i–V curves of the quartz contaminated electrolyte is the emergence of a peak in the current response in the 0.12–0.19 V region, indicating another oxidative process occurring at the electrode surface. Following this peak a discernible decrease in the normalised current response was

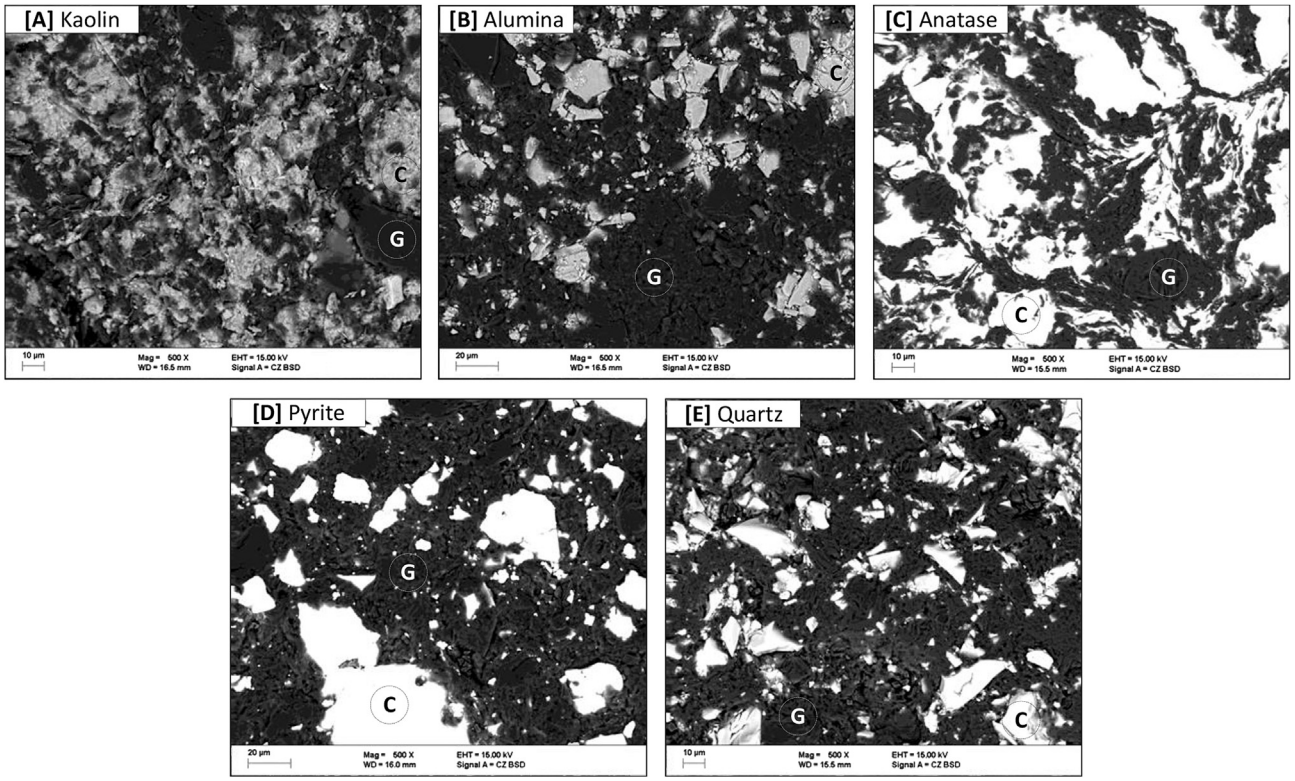

Fig. 8. SEM images (500× magnification) of working electrode surface prior to use with 50 wt% contamination of [A] kaolin, [B] alumina, [C] anatase, [D] pyrite and [E] quartz. Areas identified as graphite are indicated with a 'G' while contaminant areas are indicated with a 'C'.

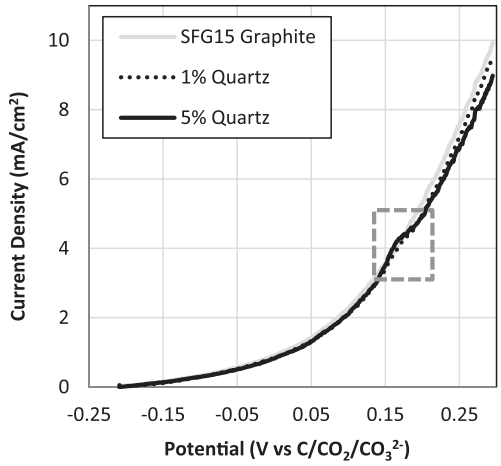

Fig. 9. LSV performed on SFG15 graphite electrode pellet using a 5 mV s^{-1} scan rate. Electrolyte contaminant loading identified in Figure and region of interest highlighted.

observed, most noticeable in the 5% contaminated electrolyte. This decrease is not significant compared to changes observed on addition of contaminants instead to the solid electrode.

4. Discussion

Results show a clear interaction of incorporated contaminants with the graphitic carbon in the case of close physical contact; i.e., combined in a solid electrode. The order of activity for contaminants tested shows increased oxidative activity in the order of kaolin > montmorillonite > alumina > anatase > pyrite. Quartz was the only contaminant tested which showed a clear decrease in the oxidative activity of the graphite. The same effects are not observed in the case of other contaminant additions and increased effects are observed for increasing inclusion of contaminants.

Similar response to increasing contaminant concentration can be seen for each contaminant added at both low and high potentials with deviations observed at higher contaminant concentrations for kaolin and montmorillonite which increase beyond response from other contaminants.

The largest enhancement observed for anode contamination was for the pre-treated kaolin, which was also shown to have the most intimate contact with graphite on mixing (Fig. 8[A]). Clear activation of the reaction occurs with increasing kaolin and montmorillonite concentrations, which is especially evident at concentrations >30 wt% in the low potential range (see Fig. 7[A]) where an apparent activation of the oxidation reaction takes place.

The cause of the activation is difficult to determine, although some authors have previously postulated ways in which the anodic oxidation of carbon could be altered mechanistically. For example, the contaminant phase could act as a mediating site for the exchange of O^{2-} species, and possibly catalyse the reaction where the phases meet. Both Li et al. [3] and Wang et al. [16] note an enhancement on the performance of their test cell when specific metal oxides were introduced to the electrolyte. Li et al., attributed performance enhancement observed for different carbon sources tested to an increase in surface oxides within the carbon phase [3]. Both kaolin and montmorillonite contain surface oxides [26] and it is possible the oxides within these structures facilitate the adsorption of O^{2-} to the electrode surface and subsequent reaction with neighbouring carbon particles.

Alternatively, the catalytic effect of the contaminants could be a result of contact between the molten electrolyte and the carbon surface. Kaolin and montmorillonite give the biggest performance enhancement when incorporated in high concentrations and were also observed to have the greatest degree of mixing and contact between the graphite and contaminants (see Fig. 8[A]). Contaminant addition may enable more intimate contact between the molten electrolyte and the carbon by changing the wettability of the electrode surface in regions where the contaminant phase is present. Contact between carbon and carbonate electrolyte was identified as a possible limitation by Chen et al. [33] and was discussed as a possibly limiting issue in a recent review paper [7].

Overall, the effect of the inclusion of quartz to the electrode surface is the most dramatic result since it appeared to almost completely inhibit the oxidation of the graphite present at high potentials (Fig. 7[B]). Given the soluble nature of quartz in the molten carbonate electrolyte [34] it is possible that the quartz contaminant is dissolving and forming a passivating layer at the electrode surface which reduces the CO_3^{2-} ion concentration in a localised area.

Devyatkin et al. [34] proposed a series of chemical equilibria that might be possible within a molten tertiary eutectic carbonate–SiO_2 mixture, some of which are predicted to occur spontaneously and under non-electrolytic conditions. The reactions proposed by Devyatkin et al. between the SiO_2 and the molten carbonate (see Eqs (5)–(7) below), mean that the intermediate species M_2SiO_3 (where M = Li, Na, K) could be present in the electrolyte at the electrode interface causing a different series of electrochemical reactions through which the carbon is oxidised; i.e.,

$$Li_2CO_3 + SiO_2 \rightarrow Li_2SiO_3 + CO_2 \qquad \Delta G = -88.48\ \text{kJ/mol} \qquad (5)$$

$$Na_2CO_3 + SiO_2 \rightarrow Na_2SiO_3 + CO_2 \qquad \Delta G = -46.48\ \text{kJ/mol} \qquad (6)$$

$$K_2CO_3 + SiO_2 \rightarrow K_2SiO_3 + CO_2 \qquad \Delta G = -39.43\ \text{kJ/mol} \qquad (7)$$

An effect of the addition of quartz to the electrolyte was also observed (Fig. 9) in the form of a small oxidative peak in the 0.12–0.19 mV region. Other impurities were not seen to have any effect on the oxidation reaction of the graphite. Li et al. [3] report a notable difference in electrochemical performance with the inclusion of only 8 wt% SiO_2 on the basis of their carbon loading (which equates to 0.6 wt% with respect to the molten carbonate electrolyte), although subtle electrochemical impacts were not able to be observed due to the particulate carbon used for oxidation. This feature in quartz contaminated carbon sources is not discussed in literature relating to coal and utilisation in the DCFC such as Li et al. [3], Cherepy et al. [17] and Vutetakis et al. [19], and is likely overshadowed by mass transport limitations of the cells used in these studies. Devyatkin et al. [34] studied the electrochemical behaviour of SiO_2 in carbonate melts utilising, amongst other electrode types, a glassy carbon electrode. On glassy carbon, the emergence of a peak is seen in the same region of the anodic voltammogram (correcting for reference electrode used and cell temperatures). Furthermore, Devyatkin et al. report no corresponding cathodic process on the working electrode during the reverse potential sweep, indicating that the process is either non-reversible or kinetically very slow. It is suggested from the literature that the process, giving rise to the peak in the anodic sweep, is due to the electrochemical oxidation of silicon carbide, which is thought to form chemically at the electrode surface during the heat-up procedure. Devyatkin et al. further confirm this with a series of experiments in which the carbon content was increased within the molten electrolyte, with reports of forming a black α-SiC coating on the working electrode. This effect could be due to the passivation of the reactive sites of the graphite surface due to SiO_2 formation.

Effects of other contaminants were not observed, contrary to results of other authors adding metal oxides to the carbonate melt [3,16]. Possibly the quiescent nature of the cell used had an effect in

this investigation for both the kaolin and montmorillonite since both the clay materials precipitated from the electrolyte, forming a solid deposit on the cell bottom and preventing the materials from coming in contact with the electrode surface.

The method and cell layout developed is shown to be effective to identifying the electrochemical effect of contaminants on a model fuel source in selected molten media. The method could further be applied in a range of applications including in the effect of contaminants present in waste derived carbon fuels and in other molten media such as sodium hydroxide and ionic liquids.

5. Conclusion

A method is outlined here which shows the ability to observe and analyse the impact of various contaminants on the oxidation reaction of carbon in a direct carbon fuel cell. This method is used to demonstrate that the inclusion of coal contaminants to the solid electrode working electrode area has a significant effect on the oxidation mechanism of a graphitic carbon model fuel and indicates the interaction and importance of coal ash on the expected performance of different coals in the direct carbon fuel cell. Clay materials appear to act as a catalyst for the oxidation of graphitic carbon while quartz can severely inhibit oxidative behaviour of the carbon. Further, it is found that small concentrations of specific ash components, when added to the carbonate electrolyte of a DCFC do not adversely impact on the oxidation reaction, although the addition of quartz will result in an additional electrochemical response within the cell.

Acknowledgements

The authors acknowledge funding from CSIRO Energy Technology for this work. ACTest Laboratories Newcastle also assisted in this work through carrying out proximate and ash analysis.

References

[1] S. Giddey, S.P.S. Badwal, A. Kulkarni, C. Munnings, Prog. Energy Combust. 38 (2012) 360–399.
[2] X. Li, Z.H. Zhu, R. De Marco, J. Bradley, A. Dicks, J. Phys. Chem. A 114 (2010) 3855–3862.
[3] X. Li, Z.H. Zhu, R. De Marco, J. Bradley, A. Dicks, J. Power Sources 195 (2010) 4051–4058.
[4] R.D. Weaver, Direct Electrochemical Generation of Electricity from Coal: Quarterly Progress Report, Stanford Research Institute, 1979.
[5] A.C. Rady, S. Giddey, S.P.S. Badwal, B.P. Ladewig, S. Bhattacharya, Energy Fuels 26 (2012) 1471–1488.
[6] D. Cao, Y. Sun, G. Wang, J. Power Sources 167 (2007) 250–257.
[7] T.M. Gür, Chem. Rev. 113 (2013) 6179–6206.
[8] X.Y. Xu, W. Zhou, F.L. Liang, Z.H. Zhu, Int. J. Hydrogen Energy 38 (2013) 5367–5374.
[9] L. Guo, J.M. Calo, E. DiCocco, E.J. Bain, Energy Fuels 27 (2013) 1712–1719.
[10] A. Elleuch, J. Yu, A. Boussetta, K. Halouani, Y. Li, Int. J. Hydrogen Energy 38 (2013) 8514–8523.
[11] B. Cantero-Tubilla, C.C. Xu, J.W. Zondlo, K. Sabolsky, E.M. Sabolsky, J. Power Sources 238 (2013) 227–235.
[12] A. Kulkarni, S. Giddey, S.P.S. Badwal, Solid State Ionics 194 (2011) 46–52.
[13] Y. Nabae, K.D. Pointon, J.T.S. Irvine, J. Electrochem. Soc. 156 (2009) B716–B720.
[14] G.A. Hackett, J.W. Zondlo, R. Svensson, J. Power Sources 168 (2007) 111–118.
[15] Y. Nabae, K.D. Pointon, J.T.S. Irvine, Energy Environ. Sci. 1 (2008) 148–155.
[16] C.Q. Wang, J. Liu, J. Zeng, J.L. Yin, G.L. Wang, D.X. Cao, J. Power Sources 233 (2013) 244–251.
[17] N.J. Cherepy, R. Krueger, K.J. Fiet, A.F. Jankowski, J.F. Cooper, J. Electrochem. Soc. 152 (2005) A80–A87.
[18] X. Li, Z.H. Zhu, R. De Marco, A. Dicks, J. Bradley, S.M. Liu, G.Q. Lu, Ind. Eng. Chem. Res. 47 (2008) 9670–9677.
[19] D.G. Vutetakis, D.R. Skidmore, H.J. Byker, J. Electrochem. Soc. 134 (1987) 3027–3035.
[20] S.S.J. Warne, Thermochim. Acta 272 (1996) 1–9.
[21] K.E. Benfell, B.B. Beamish, K.A. Rodgers, Thermochim. Acta 286 (1996) 67–74.
[22] F.J. Maldonado-Hódar, J. Rivera-Utrilla, A.M. Mastral-Lamarca, M.A. Ferro-García, Fuel 74 (1995) 818–822.
[23] F. Moodi, A.A. Ramezanianpour, A.S. Safavizadeh, Sci. Iran. 18 (2011) 906–912.
[24] G.J. Janz, M.R. Lorenz, J. Chem. Eng. Data 6 (1961) 321–323.
[25] L. Lu, V. Sahajwalla, C. Kong, D. Harris, Carbon 39 (2001) 1821–1833.
[26] M. Castellano, A. Turturro, P. Riani, T. Montanari, E. Finocchio, G. Ramis, G. Busca, Appl. Clay Sci. 48 (2010) 446–454.
[27] C.R. Ward, Int. J. Coal Geol. 50 (2002) 135–168.
[28] T. Koishi, S. Kawase, S. Tamaki, T. Ebisuzaki, J. Phys. Soc. Jpn. 69 (2000) 3291–3296.
[29] J.P. Hansen, I.R. McDonald, J. Phys. C Solid State 7 (1974) L384–L386.
[30] G.J. Janz, Molten Salts Handbook, Academic Press, New York, 1967.
[31] P.L. Spedding, R. Mills, J. Electrochem. Soc. 112 (1965) 594–599.
[32] M.F. Costa, J. Mol. Liq. 138 (2008) 61–68.
[33] M. Chen, C. Wang, X. Niu, S. Zhao, J. Tang, B. Zhu, Int. J. Hydrogen Energy 35 (2010) 2732–2736.
[34] S.V. Devyatkin, A.D. Pisanenko, V.I. Shapoval, Russ. J. Appl. Chem. 75 (2002) 562–564.